ACS APPLIED MATERIALS & INTERFACES

Research Article

www.acsami.org

Broadband and Crack-Free Antireflection Coatings by Self-Assembled Moth Eye Patterns

Francesco Galeotti,*[,†] Franco Trespidi,*[,‡] Gianluca Timò,[‡] and Mariacecilia Pasini[†]

[†]CNR Istituto per lo Studio delle Macromolecole (ISMAC), via E. Bassini 15, 20133 Milano, Italy

[‡]Ricerca sul Sistema Energetico (RSE), Strada Torre della Razza, loc. Le Mose, 29122 Piacenza, Italy

Supporting Information

ABSTRACT: We report broadband and quasi-omnidirectional antireflective (AR) structures inspired to the nipple arrays of moth eyes. These nanocoatings, based on thin elastomeric films, are prepared by simple self-assembly processing of a co-polymer specifically designed to this purpose, and PDMS replica molding. Typically, their surface is covered by a compact distribution of hemispherical nanodomes of about 250 nm in diameter and about 100 nm in height. When these novel nanostructures are applied on a single glass surface, a maximum of 2% transmission enhancement (equivalent to a 50% reduction of the reflected component) towards wavelengths ranging from visible to near IR region is obtained. A considerable AR power is observed also at a wide range of incident angles ranging from normal to 50°. These properties could be attributed to an optimized graded refractive index profile resulting from the randomly distributed and close-packed nanodomes. Moreover, thanks to their elastomeric nature, these crack-free films can be easily applied on glass, as stickers, and periodically replaced, thus offering the possibility of easy dirt removal from an optical device.

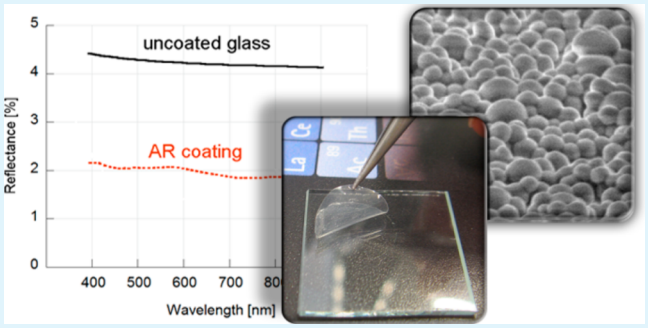

KEYWORDS: *moth eye, antireflection, nanostructures, breath figures, PDMS, nanofabrication*

INTRODUCTION

Optical devices and many energy-related applications rely on glass as a protecting barrier from external agents (such as water, humidity and other impurities) and as a transparent window for light propagation. However, the transmittance through a glass window is limited by the naturally occurring Fresnel reflection, always present at any interface separating different indices of refraction (n). Standard glass typically reflects 8% of the incoming light at a normal angle of incidence, and this percentage is even increased at higher incidence angles. Therefore, achieving higher optical transmittance in the visible and near-IR spectra by an effective antireflection (AR) coating is a key issue for overcoming some important obstacles for optoelectronic devices, such as the losses due to the surface reflection and the angular dependence of the reflectivity present also for the standard multilayer coatings in photovoltaic (PV) panels and concentration photovoltaic (CPV) systems, poor light extraction efficiency in light-emitting diodes (LEDs), and poor contrast and brightness in display devices.[1]

Up to now, two main approaches have been followed to fabricate efficient AR coatings: multilayer coatings and graded index coatings. The former approach is based on the preparation of inorganic layered thin films, which provide a reflection reduction by destructive interference of light reflected at different interfaces. The limitation of this approach is that high transmittance can be achieved only in narrow ranges of wavelength and incidence angles, which are defined by layers thickness and n values. To widen these ranges, more complicated design may be used, which usually have to be optimized by numerical algorithms, to obtain multilayers with precise control of the thickness of each layer. What is more, such coatings must be fabricated by physical vapor deposition, a process difficult to be performed on very large-size optical devices. The latter approach is the manufacturing of the so-called graded index coatings, where n is gradually varied from glass to air by the gradual variation of composition of a single layer material. This is hard to be realized, however, since n for a solid material like glass (∼1.5) is significantly different from that of air (∼1).

Observations on the corneas of nocturnal moths indicate that nature may have anticipated the solution to this problem.[2] In fact, electron microscopy studies of the corneal lenses of moths revealed that the outer surface is covered with a regular array of conical protuberances, typically about 200 nm of height and spacing, which may have the function to suppress reflections by effectively providing a graded transition of n between air and cornea tissue. These so-called nipple arrays on the surface of moth eyes allow them to see very well in the dark and at the same time eliminate glare from their eyes, preventing predators from localizing them.[3] Therefore, the realization of artificial

Received: January 31, 2014
Accepted: March 26, 2014
Published: March 26, 2014

patterns able to mimic these natural occurring surfaces, appears to be a handily solution to the problem.[4]

To make an artificial surface pattern to work properly, it is necessary that the realized nanostructures are small enough with respect to the impinging wavelengths. If we consider an ideal nanocoating composed by nanospheres, it is possible to use the Mie theory to estimate the maximum allowable diameter of the nanospheres necessary to reduce the light scattered by the coating surface thus improving the coating transmission.[5] When the diameter of one sphere is close to the wavelength, the resonant effects increase the scattered component of the radiation thus preventing a good forward transmission for all the wavelengths of the spectrum. When the sphere size becomes much smaller than the wavelength (typically sphere diameter $\ll 1$ μm) the process follows the Rayleigh model where the scattered power varies as the sixth power of the particle size, and inversely with the fourth power of the wavelength, thus reducing very much the scattered components and allowing the operation as AR coating. The Mie theory however is applicable when the spheres have all the same diameter, they are randomly distributed on the surface, and separated from each other by large distances compared to the used wavelength. On the other hand, spheres are not optimal for achieving a good AR effect because such shape would not produce a uniform effective variation between the two n (air and glass), as shown in Figure 1.

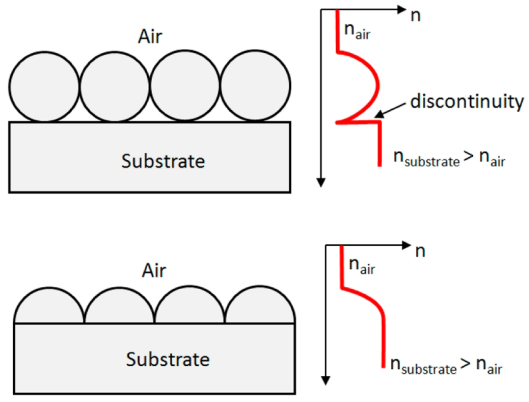

Figure 1. Schematic comparison between spherical (top) and hemispherical (bottom) nanostructures. On the right, the corresponding predicted effective refractive index profile is reported.

Therefore, nanostructures that are more similar to hemispheres are preferable in order to progressively increase the amount of solid material while approaching the glass. Moreover, poorly packed (i.e., with low area ratio) nanostructures would not produce a continuous variation of *n*, because they would not completely eliminate the *n* step at the interface between the disperse hemispheres and the substrate. For the above reasons the considerations derived from the Mie theory can be taken into account just for a preliminary assessment of the nanocoating shape.

Surface structures with different shapes, specifically realized to this aim, such as semi-pyramids,[6] nanorods,[7−9] nanocones,[10−12] nanowires,[13−15] hemispheres,[16] and nanopores,[17−21] have been recently reported by different groups. Such patterns can be produced by a number of different technologies, including epitaxial growth,[7] decal transfer lithography,[22] nanosphere lithography,[10] thermal nanoimprint lithography,[11,23] sol−gel methods,[24] block copolymers phase separation,[18,25] layer-by-layer assembly.[26−28] Among them, nanofabrication techniques that are exclusively based on the self-assembly of the materials involved, are advantageous because of the simple technology required, and thanks to their generally facile, inexpensive, and repeatable application.[29−31]

In this study, we propose an unprecedented approach to obtain a novel kind of disposable and crack-free organic nanostructured films, that can be applied by simple adhesion onto glass and operate as efficient AR coatings. For their realization in fact, we employed for the first time a fast and low-cost fabrication strategy based on breath figures (BFs) formation and replica molding.

The application of BF templates to micro and nanofabrication has been already explored in many fields.[32−34] Thin polymeric films having a distribution of micrometric cavities arranged in hexagonal fashion are in fact readily obtainable via BF process (i) through a fast (few seconds) single step approach, (ii) with no need for lithographic steps, and (iii) by means of very simple and accessible laboratory equipment. BFs can be in fact regarded as a templating method in which the template consists in the ordered array of water droplets that simply evaporate at the end of the process.[35,36] Clearly, this is convenient compared to most of the other known templating approaches, where the templates need to be removed after the use and in most of the cases they are not easily prepared or eliminated. For these reasons, BF approach is one of the most suitable methods for the fabrication of porous polymer films. The same way, replica molding is a facile and widely used technique for transferring patterns into PDMS,[37] and it has already been successfully applied to BF templates.[38]

We have recently demonstrated that elastomeric arrays of micrometric hemispherical lenses (10−20 μm of diameter) fabricated by replica molding of BFs can effectively be employed for increasing the efficiency of light extraction in organic LEDs.[39] Park et al. reported some years ago that a grading multilayer porous film prepared by BFs showed AR effect in the near-infrared regime.[40] However, to the best of our knowledge, replica molding of BFs have never been considered before as fabrication method for nanostructured broadband AR coatings, because they generally provide pore size exceeding the micrometer. Here, by making use of a properly designed templating polymer, we propose a new kind of PDMS layers decorated with sub-micrometrical features, as accessible and efficient AR coatings for glass.

2. EXPERIMENTAL SECTION

2.1. Preparation of the AR Layers. The fabrication process is schematically depicted in Figure 2. Poly[9,9-di(2-(2-tetrahydropyranyloxy) hexyl)fluorene-*alt*-9,9-dioctylfluorene] (PFOTHP) was synthesized in our laboratory by a properly controlled Suzuki polycondensation, according to a previously reported procedure.[41] 90 μL of a 1 mg mL^{-1} solution of PFOTHP in CS_2 is drop on a glass coverslip (1.5 cm side) and let evaporate under a flux of moist nitrogen (85% R.H.) at a flow rate of 150 L h^{-1}. The process is complete in 20 s, and a thin porous polymer film is left on glass (step 1). This assembly is gently covered with 40 mg of PDMS pre-polymer/curing agent mixture (Sylgard 184), an amount sufficient to obtain a film with average thickness of ~100 μm, and let rest for 1 h to allow the PDMS to fill the cavities (step 2). After this time, the substrate is baked in oven for 10 h at 60 °C. Finally, the sample is soaked in dichloromethane until the complete dissolution of the template, which releases the PDMS layer (step 3).

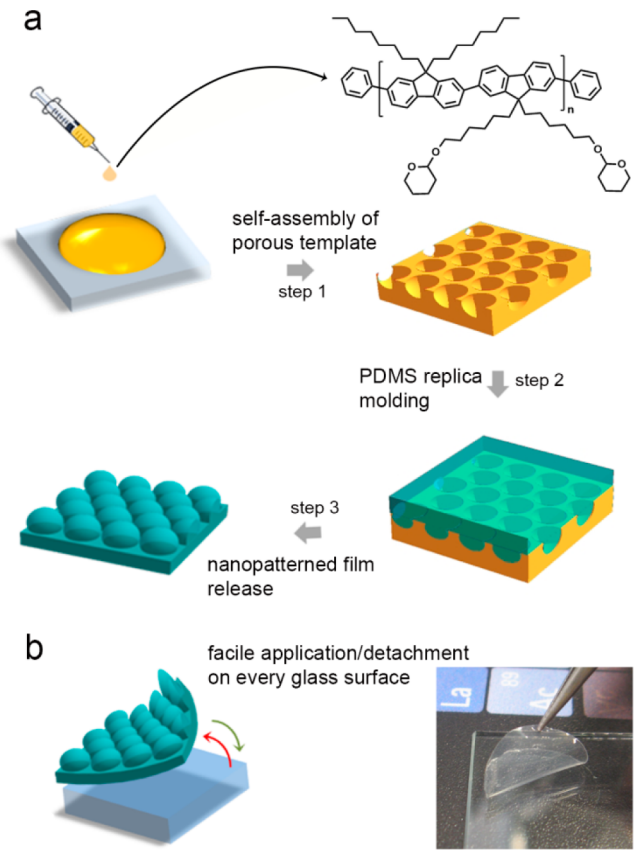

Figure 2. (a) Schematized drawing of the fabrication process. (b) Drawing and photograph of application/detachment on glass.

2.2. Characterization of the AR Layers. A white light source generating a collimated (0.6° divergence) light beam of about 5 mm in diameter is used to probe the sample. The light beam crosses the sample under test and is collected by an integrating sphere with a 9.5 mm circular input aperture. The integrating sphere is properly coupled to a spectrometer operating in the spectral range 300−1000 nm. The transmission measurement which is performed is of differential type. The nanocoating is deposited on a clean flat glass surface that acts like a movable support. A first spectral transmission measurement, which will be used as reference, is performed by measuring the glass transmission in an area where the nanocoating is not present. The glass support is then shifted to measure the transmission of the glass with the nanocoating applied on it. The percentage ratio between the two measurements, called "normalized transmission", shows the effect of the nanocoating. If the transmission is increased with respect to the uncoated glass, i.e., normalized transmission greater than 100%, it means the nanocoating is reducing the reflected component thus improving the transmission performances. The sample can be displaced at different distances from the collecting aperture of the integrating sphere so to evaluate also the presence of the scattered light. The sample can also be tilted in order to measure the performances at different incidence angles of the impinging light beam. The measurement with and without the coating are performed by moving the glass support of about 15 mm, so to minimize the errors that could be caused by the non-uniformity of the glass support. For the absolute transmission measurements, the spectra measured with the uncoated glass, with nanocoated glass and of the impinging light, were acquired separately using the same setup. The optical spectrum of the white light source coupled to the spectrometer sensitivity provided the best signal to noise ratio in the range 470−800 nm. In this spectral range, the total measurement error was evaluated to be about ±0.3%.

3. RESULTS AND DISCUSSION

3.1. Fabrication Approach. To realize nanopatterned thin layers suitable for our purpose, porous films with cavities smaller than 500 nm and with very high area ratio have to be prepared, and successively used as templates for PDMS replica molding. Even though most of the reported BF films have porosity of 1−5 μm, by this technique it is feasible to regulate the pore size to sub-micrometric size through the proper choice of the polymer and control of the casting conditions. One of the crucial points in the choice of the polymer is the presence and amount of polar groups in its structure. In fact during BF formation, the condensed water droplets are prevented to coalesce by the formation of a thin layer of solid polymer which surrounds them, and in this stabilization phenomenon the level of amphiphilicity in the polymer chains is clearly involved.[42] When the material includes a sufficient amount of hydrophilic groups, the nucleation and stabilization of a great number of water droplets is possible. If the solvent evaporation is complete before coalescence starts, very small cavities are obtained in the final film. In light of these considerations, we have developed an alternated fluorene-based block copolymer, in which the lateral alkyl chains of one of the two alternating units are terminated with the partially hydrophilic tetrahydropyranyl groups (see structure reported in Figure 2). The presence of hydrophilic pendants all along the polymer chains, and not only at the end of the chain, as in most amphiphilic materials, allows for the realization BF films of porosity smaller than 400 nm.[41] Such dimensions match the requirements for AR structures. Since in designing this material we chose to stress on the water stabilization capability, the long-range order typical of BF arrays is lost in our films. Nevertheless, a short-range (~2 μm^2) hexagonal distribution is still preserved, which is enough to guarantee a high surface coverage. We evaluated the packing of pores in these films by applying the Voronoi tessellation on SEM images, obtaining the value of entropy of conformation (S) of 0.78, which is intermediate between perfect hexagonal packing (S = 0) and random distribution (S = 1.71) (see the Supporting Information). Hence, we manufactured the AR structures as PDMS positive replicas of these porous films.

We have chosen PDMS as functional material of our AR coatings because (i) its n is very close to the one of glass, (ii) its elastomeric nature prevents the nanostructured layers from cracks, (iii) it firmly sticks to cleaned glass so that no glue is needed and periodically replacement of damaged coatings is straightforward, and (iv) it is easily processable and patternable by soft lithographic techniques. Such potential advantages of PDMS with respect to other materials (inorganic semiconductors, SiO_2, non-elastomeric polymers) are confirmed by the fact that PDMS has been recently proposed for AR applications, not only as structure-transferring medium, but also in the final device.[22,24]

Figure 2 schematically describes the preparation of a nanostructured AR layer. Initially, as reported in details in the Experimental Section, a porous film is prepared by casting a polymer solution under controlled BF conditions. Then, the PDMS AR layer is obtained by replica molding of this polymeric template. After the template is exhaustively removed by solvent dissolution, the layer appears as a thin transparent patch, which can be applied by its flat side to a glass surface, as shown in Figure 2b.

Different kinds of nanostructures, realized introducing slight variations in the fabrication process (cast volume and nitrogen

dx.doi.org/10.1021/am500687f | ACS Appl. Mater. Interfaces 2014, 6, 5827−5834

flow rate during the BF film preparation) have been tested during several months. Patterned films with hemisphere diameter exceeding 400 nm revealed to be partially ineffective, producing a strong attenuation of light transmission at the wavelengths closer to the sphere size, as indicated by the Mie theory (Mie resonant absorption). For this reason, we carefully tuned the conditions of the manufacturing technique in order to enhance the performances, as discussed later. The reason for this enhancement is ascribable to the optimized surface morphology of the layers at the nanometric scale. A comparative view of a nonperfect milky layer with an optimized nanocoating is shown in Figure 3.

Figure 3. Picture of nonperfect nanocoating (left) and good-performing nanocoating (right).

3.2. Morphology and Structure. Microscopy images of the patterned surface of an optimized AR coating, as well as the porous structure used as template (previous fabrication step), are presented in Figure 4. The template surface is covered by a closely packed arrangement of pores of 100−300 nm of diameter, with a minimal non-holed surface fraction (Figure 4a, b).

The PDMS nanocoating is the positive replica of this structure, with domes of approximately hemispherical shape in the place of pores. Because each dome is in contact with its neighbors, the roughness of the coating is smaller than the single dome height, resulting in a maximum roughness of 132 nm and an average one of 65 nm (measured by AFM, Figure 4c, d). It is important that the BF process is well-controlled in order to achieve patterns with the required quality. In fact, if the process is not fast enough, i.e., decreased moist nitrogen flow rate or increased cast volume, porosity of slightly bigger dimensions can be obtained. Specifically, we achieved a reduction of average pore diameter from 400 to 250 nm by keeping a cast volume of 90 μL and increasing the nitrogen flow rate from 50 to 150 L h^{-1}. Similarly, by keeping a nitrogen flow of 150 L h^{-1} and decreasing the cast volume from 200 to 90 μL, a reduction of pore diameter from 1 μm to 250 nm was observed (Figure 4e). On the other hand, increasing too much the evaporation speed or decreasing further the cast volume led to poorly packed or poorly homogeneously distributed domes.

3.3. Numerical Calculations. We deduced the effective refractive index (n_{eff}) gradient of the obtained nanostructures from the effective medium theory, by applying the equation proposed by Stavenga et al. for nipple arrays[43]

$$n_{\mathrm{eff}}(h) = \{\mathrm{ff}(h)n_{\mathrm{PDMS}}^{q} + [1 - \mathrm{ff}(h)]n_{\mathrm{air}}^{q}\}^{1/q} \quad (1)$$

where q is 2/3, n_{PDMS} and n_{air} are respectively the refractive index of PDMS and air, and ff(h) is the fill factor, defined as the area ratio of the nanodomes to the total substrate surface at height (h), which was obtained from the AFM analysis. Figure 5 shows the calculated n_{eff} for two different wavelengths. A full AFM image and some examples of its planar sections taken at different h, are also shown. These sections were used for evaluating the $ff(h)$ values. The plot clearly shows that the nanocoating is able to provide a gradual variation of n_{eff} from air to PDMS substrate, the only residual step being due to the n difference between PDMS and glass. Compared to the calculated n_{eff} variation for an ideal array of hemispheres of the same size (as the one schematized in Figure 1 bottom), reported in dashed lines in Figure 5, the real nanocoating behaves even more efficiently, since it is able to suppress the n step at h = 0, because of the fill factor geometrical limit (for more details, see the Supporting Information). We can explain

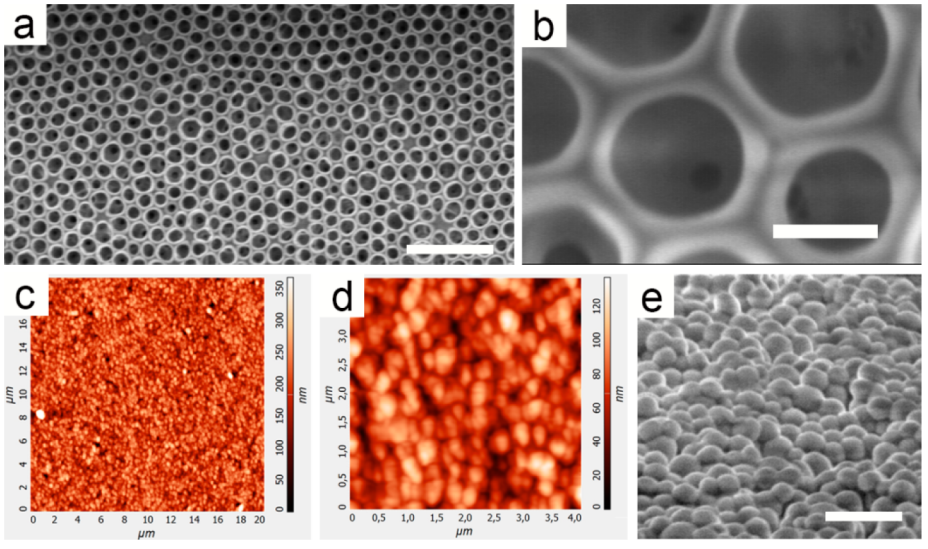

Figure 4. (a, b) Top-view SEM image of the nanoporous film used as template for nanocoating, at different magnifications. Scale bars are 2 μm and 200 nm, respectively. (c, d) AFM images of the nanocoating, at different magnifications. (e) SEM tilted view of the nanocoating. Scale bar is 1 μm.

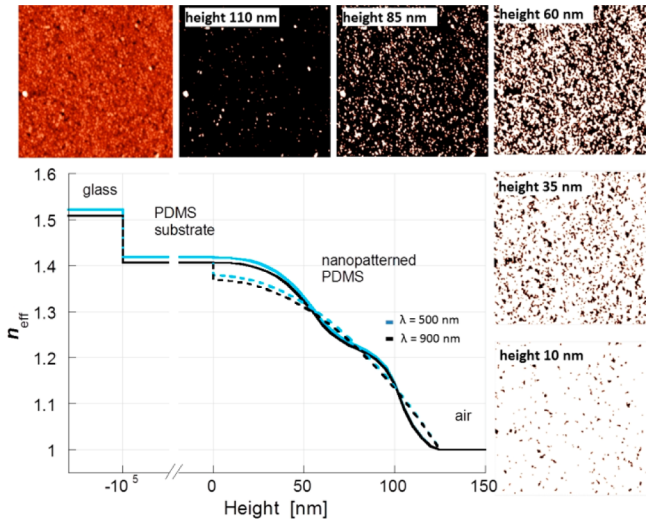

Figure 5. Comparison between the real (solid line) and theoretical (dashed line) effective index of refraction profiles of the nanocoating, from glass to air. The two curves were respectively obtained from the analysis of the AFM image of the nanostructure (line) and supposing a hexagonal packing of ideal hemispheres (dashed line). Full AFM image of the nanocoating and some examples of planar sections at different heights, used for this calculation, are also shown.

this effect with the fact that, thanks to our approach, in the real nanocoating, the hemispheres have slightly different sizes and shapes, so that a superior packing with respect to the ideal case is possible.

The grading n_{eff} ability of these nanostructures, estimated on the basis of their shape, will be shown to play an important role in suppressing the undesired reflectance.

3.4. Antireflection Properties. As light passes through a glass window, its total impinging power splits into different contributions: reflected, transmitted, absorbed, forward scattered, and backward scattered. While for a smooth and transparent surface such as naked glass, the first two contributions are the most relevant ones, in a more complex system such as glass coated by a patterned layer, all the contributions must be taken into account. For this reason, we evaluated the performances of the manufactured AR nanocoatings by performing transmission measurements. In this contest in fact, transmission is more significant than reflectivity, since the former is a direct measurement of the amount of light which effectively passes through glass, so that it can reach (or be extracted by) the device. We also want to remark, for a correct comprehension of the results, that some of the studies published in this field consider both surfaces coated by an AR system, so that the final AR effect is doubled. Our aim is to focus on the application of the nanocoating to the external window of an optical device; hence, we here considered only one coated surface, because in the real case the second face would be in contact with the device surface.

In Figure 6a, the normalized transmission (previously explained) of some PDMS nanocoatings with respect to an uncoated glass surface is reported. The ratio between the two measurements shows the effect of the nanocoating. Where the normalized transmission is higher than 100%, the nanocoating is improving the transmission performances of the uncoated glass, thus reducing the reflected component. Conversely, for values lower than 100%, the coating is reducing the light transmitted through glass window.

These measurements are obtained by placing the coated glass close to the input area of the integrating sphere used to collect the radiation after the sample. An example of a non-optimized pattern is provided by curve 2, where light attenuation for wavelength smaller than 420 nm is clearly visible. Similar attenuation of light transmission was observed when the hemisphere size was comparable to the impinging wavelength. After morphology optimization, the nanopatterned layers showed an increase in the light transmission of more than

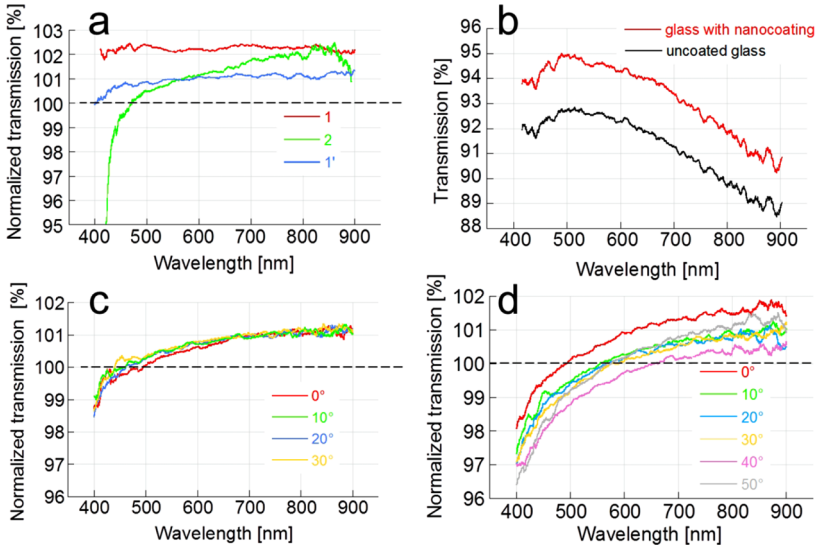

Figure 6. (a) Transmission of PDMS nanocoating normalized in percentage to the transmission of an uncoated glass surface (normalized transmission), placed at 0 cm from the collecting area for an incidence angle of 0° (curve 1); same measurement performed on a nonperfect nanocoating (curve 2), and on the first coating after six months of ageing (curve 1′). (b) Comparison between absolute transmissions of an uncoated glass and a glass with the PDMS nanocoating applied on a single surface at normal incidence. (c) Normalized transmission at 1 cm from the collecting area, for incidence angles in the range 0−30°. (d) Normalized transmission at 5 cm from the collecting area, for incidence angles in the range 0−50°.

dx.doi.org/10.1021/am500687f | ACS Appl. Mater. Interfaces 2014, 6, 5827−5834

2% over a single glass surface (curve 1). When the coated glass was brought at a certain distance from the collecting area, we observed a reduction of the performances (not shown). This confirms that part of the light transmitted by the coating is due to the scattered components which are not collected when the sample is far from the collecting area. However, the purpose of the coating is to increase the transmission of the optical windows, so in this case also the amount of light scattered from the surface must be included in the optical balance.

In order to visualize a direct comparison between naked glass and glass coated on one surface, we plotted also their respective absolute transmissions (Figure 6b). The lower transmission at longer wavelengths for both curves is due to the glass absorption caused by some residual impurities of Fe_2O_3 impurities.

As shown here, the application of the AR nanocoating on one face of the glass enhances its transmission of 2% over the whole spectral range. The maximum transmission is reached at 500 nm, where values of 92.8% and 95% for the uncoated and the coated glass, respectively, are recorded.

Further tests have been performed to characterize the coating at different incidence angles of the impinging beam, and the results are summarized by plots c and d in Figure 6. Intriguingly, the transmission is not significantly affected by the incidence angle (Figure 6c), meaning that the nanocoating is capable of minimizing the light reflection on glass that usually increases with the incidence angle. The dependence on the angle of incidence becomes evident when the sample is quite far from the collecting area (5 cm) thus preventing the scattered light to be collected by the input aperture of the integrating sphere. By using this setup the shorter wavelengths, which are scattered at higher angles, cannot be collected, as expected by the scattering theory. In that case the performances with respect to an uncoated glass surface placed in the same position progressively deteriorate until an angle of 40°, whereas an improvement is observed at 50°, as shown in Figure 6d. This latter observation is most probably due to the fact that the behavior of the uncoated glass surface used as reference is approaching the total internal reflection (TIR) angle for glass. Because the nanostructured surface does not suffer from TIR as a flat surface, the transmission of the coated case is not reduced as strongly as for the uncoated case, hence the normalized transmission increases when approaching the TIR angle. The better performances observed in the IR region can be explained because in such spectral region the size of the nanospheres can be considered much smaller with respect to the impinging wavelengths, so they act more efficiently.

To properly evaluate the performances achieved, they have to be compared with the typical response of an uncoated glass and with the performances of standard commercial coatings.

The typical Fresnel reflection of an uncoated glass surface, referred to unpolarized light, is shown in Figure 7 (black line).[44] The reflected light is slightly higher than 4% of the total impinging light. As discussed above, by using an optimized nanocoating, a 2% increase in the glass average transmission was observed here for a single glass/air surface, considering both the optical polarizations and in the visible/near IR spectrum (400−900 nm).

Therefore, such 2% improvement means a 50% reduction of the reflected component. To visualize it in the same reflectance plot, we reported the performance of the realized PDMS nanocoating (red dotted line) by assuming that the contribution of both adsorbed and scattered light is equal to zero, hence we consider back reflection as the only phenomenon responsible for the entire transmission loss. This is obviously an approximation, useful to make a direct comparison of performances. As discussed above, the real reflectivity of the PDMS coating is most likely lower than this value.

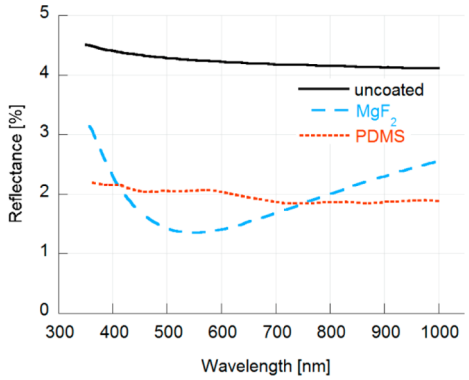

Figure 7. Single surface reflection curves taken at normal incidence for uncoated glass (black line), typical MgF_2 reflection curve (blue dashed line), and patterned PDMS coated glass (red dotted line).

One of the most common high-performance broadband coatings is MgF_2. This is a single layer coating that, when optimized for the visible spectrum, exhibits an excellent AR power, as shown by the blue dashed curve in Fig. 7. As it can be noticed, MgF_2 produces a minimum value of reflectivity of 1.3%, but this value becomes higher than 2% at the edges of the spectral range. Moreover such coating is sensitive to the incidence angle and even its minimum reflectivity becomes greater than 2% at an incidence angle of 45°.[45] The same limitation is provided by commercial multilayer coatings. In fact, the reflection of such coatings rapidly increases at the edges of the spectral range and they are also very sensitive to the incidence angle. In comparison, the manufactured nanopatterned layers exhibit an excellent behavior in terms of both efficacy at the spectral edges and low sensibility to the incidence angle. In particular, it is worth noticing that the performances of our PDMS AR coating clearly overtake commercial MgF_2 in the near IR spectral region. Considering that a great effort is being made nowadays to enhance the PV systems efficiency specifically in the near IR portion of solar spectrum,[46] our AR coatings are able to fit the development in this field.

The nanocoating performances were tested again after keeping them in the laboratory, under the action of light and dust, for a period of six months, to evaluate possible ageing effects. After this time, the average transmission was still better than the naked glass (see Figure 6a, curve 1′). It is important to emphasize that PDMS is one of the most resistant polymeric materials; its salient properties include thermal and oxidative stability, resistance to weathering, low surface tension, high resistivity, and chemical and biological inertness.[47,48] We ascribe the observed efficiency reduction as due to dust accumulation and repeated manipulation of the samples. Microscopy analysis of the aged samples confirmed that, apart from augmented superficial dirt, surface morphology is comparable to fresh samples. Because such a kind of coating is cheap and easy to remove and replace, like a sticker, this last observation suggests that it can be used as AR and protective anti-dust coating for at least six months, and then be replaced by a new one. The coatings are currently subjected to tests under standard conditions of use for longer periods.

4. CONCLUSIONS

In conclusion, we have successfully applied the BF approach to obtain a new elastomeric AR coating comprising hemispheres having an average size smaller than 300 nm. It was possible thanks to a properly synthesized templating polymer, by means of a cheap and easy self-assembly technique. This nanostructured material applied on a glass surface improves the transmission at normal incidence of more than 2% in the 400−900 nm spectral range, which corresponds to a 50% reduction of the reflected component, thus demonstrating its potential as graded index nanocoating. After 6 months, a transmission improvement of at least 1% is retained. The coating exhibits also a considerable AR power at different incidence angles.

The proposed fabrication technique relies on the use of the BF methodology, a self-assembly process that is advantageous in terms of costs and realization handiness, but it is also scalable to industrial production, as proved by the recent realization of large scale fabrication prototypes.[49] The main efforts are now devoted to reduce the size of the patterning in order to improve further the transmission performances, to investigate the effect of aging and to study the consequence of a certain degree of randomization in the sizes and distribution of the hemispheres by using proper simulation software. Indeed the efficacy of our coatings may be also due to the fact that these nanostructures lack of a long range distribution order, similar to the nipple arrays of moth eyes.[3] Such controlled disorder, which is not easily achievable with electron beam or laser lithographic processes, is probably the reason why our nanocoatings provide a more gradual n variation than in the case of a perfect hemisphere array.

Further studies shall also investigate the coating damage threshold, which is an important parameter in high light intensity applications such as CPV.

Because these patterned films are affordable with a low-cost and low-technology manufacturing process, and given the easy application and replacement of these sticky elastic patches to glass surface, we propose our AR nanocoating as a practical solution for both LED and PV system applications.

■ ASSOCIATED CONTENT

Supporting Information

Evaluation of pore packing by Voronoi polygons, numerical calculation details, and description of the optical setup. This material is available free of charge via the Internet at http://pubs.acs.org.

■ AUTHOR INFORMATION

Corresponding Authors

*E-mail: f.galeotti@ismac.cnr.it.

*E-mail: franco.trespidi@rse-web.it.

Notes

The authors declare no competing financial interest.

■ ACKNOWLEDGMENTS

We thank Dr. T. Virgili (CNR-IFN) for her careful and critical reading of our paper. This work was supported by CARIPLO project EDHONIST (ref. 2012-0844), by the project Regione Lombardia (decreto 3667/2013) "Tecnologie e materiali per l'utilizzo efficiente dell'energia solare" and by the Research Fund for the Italian Electrical System under the Contract Agreement between RSE SpA and the Ministry of Economic Development, General Directorate for Nuclear Energy, Renewable Energy, and Energy Efficiency, in compliance with the Decree of March 8, 2006.

■ REFERENCES

(1) Raut, H. K.; Ganesh, V. A.; Nair, A. S.; Ramakrishna, S. Anti-Reflective Coatings: A Critical, in-Depth Review. *Energy Environ. Sci.* **2011**, *4*, 3779−3804.

(2) Clapham, P. B.; Hutley, M. C. Reduction of Lens Reflexion by the "Moth Eye" Principle. *Nature* **1973**, *244*, 281−282.

(3) Vukusic, P.; Sambles, J. R. Photonic Structures in Biology. *Nature* **2003**, *424*, 852−855.

(4) Leem, J. W.; Song, Y. M.; Yu, J. S. Biomimetic Artificial Si Compound Eye Surface Structures with Broadband and Wide-Angle Antireflection Properties for Si-Based Optoelectronic Applications. *Nanoscale* **2013**, *5*, 10455−10460.

(5) Born, M.; Wolf, E. *Principles of Optics: Electromagnetic Theory of Propagation, Interference and Diffraction of Light*, 7th ed.; Cambridge University Press: Cambridge, U.K., 1999.

(6) Woo, J. C.; Baek, N. S.; Kim, J. Y.; Kim, C. I. The Periodically Negative Semi-Pyramid Nanostructured Polymer Layer for Broadband Anti-Reflection Effect. *RSC Adv.* **2012**, *2*, 7677−7680.

(7) Diedenhofen, S. L.; Vecchi, G.; Algra, R. E.; Hartsuiker, A.; Muskens, O. L.; Immink, G.; Bakkers, E. P. A. M.; Vos, W. L.; Rivas, J. G. Broad-Band and Omnidirectional Antireflection Coatings Based on Semiconductor Nanorods. *Adv. Mater.* **2009**, *21*, 973−978.

(8) Cai, J.; Ye, J.; Chen, S.; Zhao, X.; Zhang, D.; Chen, S.; Ma, Y.; Jin, S.; Qi, L. Self-Cleaning, Broadband and Quasi-Omnidirectional Antireflective Structures Based on Mesocrystalline Rutile Tio2 Nanorod Arrays. *Energy Environ. Sci.* **2012**, *5*, 7575−7581.

(9) Lin, Y. R.; Lai, K. Y.; Wang, H. P.; He, J. H. Slope-Tunable Si Nanorod Arrays with Enhanced Antireflection and Self-Cleaning Properties. *Nanoscale* **2010**, *2*, 2765−2768.

(10) Park, H.; Shin, D.; Kang, G.; Baek, S.; Kim, K.; Padilla, W. J. Broadband Optical Antireflection Enhancement by Integrating Antireflective Nanoislands with Silicon Nanoconical-Frustum Arrays. *Adv. Mater.* **2011**, *23*, 5796−5800.

(11) Choi, K.; Park, S. H.; Song, Y. M.; Cho, C.; Lee, H. S. Robustly Nano-Tailored Honeycomb Structure for High-Throughput Antireflection Polymer Films. *J. Mater. Chem.* **2012**, *22*, 17037−17043.

(12) Ji, S.; Song, K.; Nguyen, T. B.; Kim, N.; Lim, H. Optimal Moth Eye Nanostructure Array on Transparent Glass Towards Broadband Antireflection. *ACS Appl. Mater. Interfaces* **2013**, *5*, 10731−10737.

(13) Dai, Y. A.; Chang, H. C.; Lai, K. Y.; Lin, C. A.; Chung, R. J.; Lin, G. R.; He, J. H. Subwavelength Si Nanowire Arrays for Self-Cleaning Antireflection Coatings. *J. Mater. Chem.* **2010**, *20*, 10924−10930.

(14) Chang, H. C.; Lai, K. Y.; Dai, Y. A.; Wang, H. H.; Lin, C. A.; He, J. H. Nanowire Arrays with Controlled Structure Profiles for Maximizing Optical Collection Efficiency. *Energy Environ. Sci.* **2011**, *4*, 2863−2869.

(15) Chao, Y. C.; Chen, C. Y.; Lin, C. A.; He, J. H. Light Scattering by Nanostructured Anti-Reflection Coatings. *Energy Environ. Sci.* **2011**, *4*, 3436−3441.

(16) Linn, N. C.; Sun, C. H.; Jiang, P.; Jiang, B. Self-Assembled Biomimetic Antireflection Coatings. *Appl. Phys. Lett.* **2007**, *91*, 101108-1−101108-3.

(17) Joo, W.; Kim, H. J.; Kim, J. K. Broadband Antireflection Coating Covering from Visible to near Infrared Wavelengths by Using Multilayered Nanoporous Block Copolymer Films. *Langmuir* **2009**, *26*, 5110−5114.

(18) Li, X.; Gao, J.; Xue, L.; Han, Y. Porous Polymer Films with Gradient-Refractive-Index Structure for Broadband and Omnidirectional Antireflection Coatings. *Adv. Funct. Mater.* **2010**, *20*, 259−265.

(19) Liu, L. Q.; Wang, X. L.; Jing, M.; Zhang, S. G.; Zhang, G. Y.; Dou, S. X.; Wang, G. Broadband and Omnidirectional, Nearly Zero Reflective Photovoltaic Glass. *Adv. Mater.* **2012**, *24*, 6318−6322.

(20) Walheim, S.; Schaffer, E.; Mlynek, J.; Steiner, U. Nanophase-Separated Polymer Films as High-Performance Antireflection Coatings. *Science* **1999**, *283*, 520−522.

(21) Leem, J. W.; Yu, J. S. Multi-Functional Antireflective Surface-Relief Structures Based on Nanoscale Porous Germanium with Graded Refractive Index Profiles. *Nanoscale* **2013**, *5*, 2520−2526.
(22) Bowen, A. M.; Motala, M. J.; Lucas, J. M.; Gupta, S.; Baca, A. J.; Mihi, A.; Alivisatos, A. P.; Braun, P. V.; Nuzzo, R. G. Triangular Elastomeric Stamps for Optical Applications: Near-Field Phase Shift Photolithography, 3d Proximity Field Patterning, Embossed Antireflective Coatings, and Sers Sensing. *Adv. Funct. Mater.* **2012**, *22*, 2927−2938.
(23) Raut, H. K.; Dinachali, S. S.; He, A. Y.; Ganesh, V. A.; Saifullah, M. S. M.; Law, J.; Ramakrishna, S. Robust and Durable Polyhedral Oligomeric Silsesquioxane-Based Anti-Reflective Nanostructures with Broadband Quasi-Omnidirectional Properties. *Energy Environ. Sci.* **2013**, *6*, 1929−1937.
(24) Zhang, X. X.; Xia, B. B.; Ye, H. P.; Zhang, Y. L.; Xiao, B.; Yan, L. H.; Lv, H. B.; Jiang, B. One-Step Sol-Gel Preparation of Pdms-Silica Ormosils as Environment-Resistant and Crack-Free Thick Antireflective Coatings. *J. Mater. Chem.* **2012**, *22*, 13132−13140.
(25) Sim, D. M.; Choi, M. J.; Hur, Y. H.; Nam, B.; Chae, G.; Park, J. H.; Jung, Y. S. Ultra-High Optical Transparency of Robust, Graded-Index, and Anti-Fogging Silica Coating Derived from Si-Containing Block Copolymers. *Adv. Opt. Mater.* **2013**, *1*, 428−433.
(26) Du, Y.; Luna, L. E.; Tan, W. S.; Rubner, M. F.; Cohen, R. E. Hollow Silica Nanoparticles in Uv−Visible Antireflection Coatings for Poly(Methyl Methacrylate) Substrates. *ACS Nano* **2010**, *4*, 4308−4316.
(27) Wu, Z.; Walish, J.; Nolte, A.; Zhai, L.; Cohen, R. E.; Rubner, M. F. Deformable Antireflection Coatings from Polymer and Nanoparticle Multilayers. *Adv. Mater.* **2006**, *18*, 2699−2702.
(28) Cebeci, F. Ç.; Wu, Z.; Zhai, L.; Cohen, R. E.; Rubner, M. F. Nanoporosity-Driven Superhydrophilicity: A Means to Create Multifunctional Antifogging Coatings. *Langmuir* **2006**, *22*, 2856−2862.
(29) Zhang, J. H.; Li, Y. F.; Zhang, X. M.; Yang, B. Colloidal Self-Assembly Meets Nanofabrication: From Two-Dimensional Colloidal Crystals to Nanostructure Arrays. *Adv. Mater.* **2010**, *22*, 4249−4269.
(30) Sakakibara, K.; Hill, J. P.; Ariga, K. Thin-Film-Based Nanoarchitectures for Soft Matter: Controlled Assemblies into Two-Dimensional Worlds. *Small* **2011**, *7*, 1288−1308.
(31) Askar, K.; Phillips, B. M.; Fang, Y.; Choi, B.; Gozubenli, N.; Jiang, P.; Jiang, B. Self-Assembled Self-Cleaning Broadband Anti-Reflection Coatings. *Colloids Surf., A* **2013**, *439*, 84−100.
(32) Escalé, P.; Rubatat, L.; Billon, L.; Save, M. Recent Advances in Honeycomb-Structured Porous Polymer Films Prepared Via Breath Figures. *Eur. Polym. J.* **2012**, *48*, 1001−1025.
(33) Hernandez-Guerrero, M.; Stenzel, M. H. Honeycomb Structured Polymer Films Via Breath Figures. *Polym. Chem UK* **2012**, *3*, 563−577.
(34) Srinivasarao, M.; Collings, D.; Philips, A.; Patel, S. Three-Dimensionally Ordered Array of Air Bubbles in a Polymer Film. *Science* **2001**, *292*, 79−83.
(35) Bolognesi, A.; Mercogliano, C.; Yunus, S.; Civardi, M.; Comoretto, D.; Turturro, A. Self-Organization of Polystyrenes into Ordered Microstructured Films and Their Replication by Soft Lithography. *Langmuir* **2005**, *21*, 3480−3485.
(36) Stenzel, M. H.; Barner-Kowollik, C.; Davis, T. P. Formation of Honeycomb-Structured, Porous Films Via Breath Figures with Different Polymer Architectures. *J. Polym. Sci., Part A: Polym. Chem.* **2006**, *44*, 2363−2375.
(37) Xia, Y.; Whitesides, G. M. Soft Lithography. *Angew. Chem., Int. Ed.* **1998**, *37*, 550−575.
(38) Yabu, H.; Shimomura, M. Simple Fabrication of Micro Lens Arrays. *Langmuir* **2005**, *21*, 1709−1711.
(39) Galeotti, F.; Mroz, W.; Scavia, G.; Botta, C. Microlens Arrays for Light Extraction Enhancement in Organic Light-Emitting Diodes: A Facile Approach. *Org. Electron.* **2013**, *14*, 212−218.
(40) Park, M. S.; Kim, J. K. Broad-Band Antireflection Coating at near-Infrared Wavelengths by a Breath Figure. *Langmuir* **2005**, *21*, 11404−11408.
(41) Bolognesi, A.; Galeotti, F.; Moreau, J.; Giovanella, U.; Porzio, W.; Scavia, G.; Bertini, F. Unsoluble Ordered Polymeric Pattern by Breath Figure Approach. *J. Mater. Chem.* **2010**, *20*, 1483−1488.
(42) Muñoz-Bonilla, A.; Fernández-García, M.; Rodríguez-Hernández, J. Towards Hierarchically Ordered Functional Porous Polymeric Surfaces Prepared by the Breath Figures Approach. *Prog. Polym. Sci.* **2014**, *39*, 510−554.
(43) Stavenga, D. G.; Foletti, S.; Palasantzas, G.; Arikawa, K. Light on the Moth-Eye Corneal Nipple Array of Butterflies. *Proc. R. Soc. B* **2006**, *273*, 661−667.
(44) Data available from optical components producer at: http://alexis.jtlnet.com/~escoprod/escoproducts.com/html/single_layer_mgf2_coatings.html.
(45) See as an example: http://www.cvimellesgriot.com/products/Documents/TechnicalGuide/Antireflection_Coatings_CVIMG.pdf.
(46) Ameri, T.; Khoram, P.; Min, J.; Brabec, C. J. Organic Ternary Solar Cells: A Review. *Adv. Mater.* **2013**, *25*, 4245−4266.
(47) Tomer, N.; Delor-Jestin, F.; Frezet, L.; Lacoste, J. Oxidation, Chain Scission and Cross-Linking Studies of Polysiloxanes Upon Ageings. *Open J. Org. Polym. Mater.* **2012**, *2*, 13−22.
(48) Drake, R.; MacKinnon, I.; Taylor, R. Recent Advances in the Chemistry of Siloxane Polymers and Copolymers. In *Patai's Chemistry of Functional Groups*; John Wiley & Sons: New York, 2009.
(49) Iwanaga, H.; Shiratsuchi, K.; Yamazaki, H. Fabrication and Application of Honeycomb Film. In *FUJIFILM Research & Development Report No. 54*; FUJIFILM: Tokyo, 2009; pp 43−47.